



## Fatigue performance of superelastic NiTi near stress-induced martensitic transformation



Eduardo Alarcon <sup>a,b</sup>, Luděk Heller <sup>b,\*</sup>, Shabnam Arbab Chirani <sup>a</sup>, Petr Šittner <sup>b</sup>, Jaromír Kopeček <sup>b</sup>, Luc Saint-Sulpice <sup>a</sup>, Sylvain Calloch <sup>c</sup>

<sup>a</sup> ENI Brest, FRE CNRS 3744, IRDL, F-29200 Brest, France

<sup>b</sup> Institute of Physics, Czech Academy of Sciences, Na Slovance 1999/2, 182 21 Prague 8, Czech Republic

<sup>c</sup> ENSTA Bretagne, FRE CNRS 3744, IRDL, F-29200 Brest, France

### ARTICLE INFO

#### Article history:

Received 7 July 2016

Received in revised form 2 October 2016

Accepted 5 October 2016

Available online 6 October 2016

#### Keywords:

Shape memory alloys

Nitinol

Superelasticity

Martensitic transformation

Fatigue

### ABSTRACT

The structural fatigue of superelastic NiTi was studied with special attention paid to the drop in fatigue performance commonly observed at the onset of the stress-induced martensitic transformation. We processed the superelastic NiTi wires into an hourglass shape as a result of which the stress induced martensitic transformation in tension is not localized as confirmed by digital image correlation measurements. The hourglass shaped samples were subjected to force controlled pull-pull fatigue tests at two distinct temperatures selected to investigate the fatigue of NiTi with and without the R-phase transformation involved, and to capture the effect of varying critical stress for the onset of B19' martensitic transformation. Resulting fatigue curves expressed in terms of both the stress and the strain show a first degradation of fatigue performance at stresses more than 200 MPa below the onset of the martensitic transformation. Furthermore, fatigue curves showed a temperature dependence which was successfully implemented into a modified Basquin's power law model. Notably, the fatigue life drops down to  $10^4$  cycles before the nominal loadings reach the B19' transformation regime. We further found that fatigue life is shorter for the B2-R-phase transformation regime than for the elasticity of the parent B2 austenite phase at low stresses when strains remain below 1%, however at higher strains the B2-R-phase transforming wire is better than the elastic one. Fatigue crack observations revealed crack initiation at the surface and its propagation towards the bulk resulting in a reduction of the cross-section and substantial increase in normal stresses. Martensitic transformation was triggered during the crack growth in samples nominally loaded in elastic or R-phase transformation regimes as confirmed by in-situ infrared thermography. As the crack grows with increasing speed, the activity of transformation processes at the tip gradually increases till unstable crack growth and final rupture occurs, as confirmed by in-situ thermography and stress hysteresis observations. The analysis of fracture surfaces revealed five different crack growth regimes - from quasi-cleavage at early crack growth, through propagation stage evidenced by striations, till the final ductile fracture evidenced by the typical fracture surface morphology.

© 2016 Elsevier Ltd. All rights reserved.

## 1. Introduction

NiTi based shape memory alloys display an attractive combination of mechanical properties, biocompatibility, corrosion resistance and unique functional properties such as thermally induced recovery of large strains and deflections (shape memory effect), large cyclic mechanical energy absorption (vibration damping) and large reversible deformations up to 10% (superelasticity) [1]. These properties predetermine NiTi alloys for use in medical devices, actuators, mechanical dampers [2]. The superelasticity of

NiTi is achieved through a reversible stress-induced martensitic transformation [3]. In simple words, when a critical elastic stress is reached, for instance in a NiTi wire subjected to tension, the initial B2 cubic phase termed austenite transforms without diffusion into the B19' monoclinic phase termed martensite being up to 10% longer. In addition, an intermediate transformation to triclinic R-phase accompanied with a lower ~0.5% transformation strain may occur. Upon unloading the wire shrinks to its initial length through a reverse transformation back to the austenite. Unfortunately, wider use of cyclic superelasticity in NiTi has been so far hindered by poor structural fatigue performance that drops down to few thousands cycles whenever large recoverable strains are employed in engineering applications [4–6].

\* Corresponding author.

E-mail address: [heller@fzu.cz](mailto:heller@fzu.cz) (L. Heller).

Attracted by high application potential of NiTi alloys, researchers began to investigate the fatigue behavior of NiTi alloys soon after their discovery in early sixties of 20th century [7–9]. The fatigue behavior has been addressed with respect to complex constitutive behavior of NiTi alloys, which is highly non-linear, temperature dependent, and involving thermomechanically induced transformations between the austenite and martensite phases. Therefore, fatigue studies have focused high cycle fatigue endurance of individual phases as well as low cycle fatigue in the regime of cyclic phase transformation [10–15]. Crystallographic rules governing the phase transformation and their consequences for the fatigue damage motivated researchers to perform fatigue studies on single crystalline samples [16,17]. Nevertheless, most of experimental data in the literature concern fatigue of polycrystalline NiTi semi-products [10–15]. Specifically, fatigue of thin superelastic NiTi wires with diameters below 0.5 mm has been frequently investigated as these wires are widely used in medical applications. Experimentally, the fatigue of NiTi alloys has been investigated using Stress-N, Strain-N, and damage tolerant approaches. The Strain-N approach has been preferred over the Stress-N in studies of low-cycle fatigue in highly non-linear phase transformation regime where large strains appear at nearly constant stresses or temperatures. Rotary bending and tensile loading are preferred techniques for fatigue testing of superelastic NiTi wires. Recently, the issue of amount of inclusions and its effect on fatigue life has been addressed as a response to the problem of fatigue failures of medical graded superelastic NiTi wires initiated near surface located inclusions [18]. Likewise, corrosion-fatigue and the use of electrochemical potential to track the surface damage leading to early crack nucleations have been studied thus addressing the fatigue of superelastic stents exposed to harsh body fluids environments [19,20]. Finally, findings of a large body of literature dealing with fatigue of NiTi published over decades have been recently summarized in a few review publications [4–6], which the reader may refer to for a detailed state-of-the art.

As stated in review [4], fatigue prediction strategies for superelastic NiTi alloys are not yet available as the constitutive behavior of NiTi alloys is complex and mechanisms of their fatigue damage are not fully understood. Nevertheless, several methods have been suggested in the literature to assess the fatigue performance of superelastic NiTi alloys. Among others, constant life diagrams for various strain amplitudes and mean strains constructed for superelastic NiTi components have been suggested [21]. Within damage tolerant approaches, Kitagawa diagram has been used to depict limiting conditions for cyclic fatigue failure of superelastic thin-walled NiTi tubes [22]. Furthermore, Strain-N diagrams combining fatigue data obtained from various multiaxial loadings have been used [4]. Results of low-cycle multiaxial fatigue testing in the phase transformation regime were represented by graphs of equivalent transformation strain amplitude vs. number of cycles in order to fit a modified Coffin-Manson relationship developed for low-cycle fatigue in the regime of plastic deformation. Similarly, Maletta et al. [23] suggested to estimate the fatigue life of phase transforming superelastic NiTi using a modified Coffin-Manson approach where inelastic deformation through phase transformation is considered instead of the plastic strain. To sum up, various approaches are being currently applied to deal with the fatigue of NiTi alloys. Some of them have been derived from tools and methods that had been developed earlier for elasto-plastic materials. Thus, they cannot accurately reflect the deformation and irreversible processes that are unique to NiTi shape memory alloys such as large reversible transformation strain, temperature dependency of the critical stress for the onset of martensitic transformation, and transformation induced plasticity. Inevitably, we have to try to better understand how these processes affect the fatigue behavior of NiTi in terms of microstructure changes, crack initiation and

growth. This knowledge will provide a basis for development of fatigue prediction models and tools.

In this work, we investigate the critical drop in fatigue performance of medical graded superelastic NiTi wires when the loading approaches the regime of the stress-induced martensitic transformation allowing for large recoverable strains (superelasticity). This drop has been evidenced by a number of experimental works [4–6,18,24–27]. In spite of that it represents a key issue, its origin remains unclear. Minor improvements in fatigue performance can be achieved using a proper selection of degree of cold work, thermal treatment conditions, and degree of alloy impurities [18,25–27]. The transition from millions of cycles to few thousands in NiTi wires loaded in tensile tests with increasing strain (stress) amplitudes has never been focused in fatigue studies since it is largely hindered by the strain localization of NiTi in tension [28,29]. There is no continuous homogenous tensile straining of the NiTi wire when the martensitic transformation regime is reached. Instead, the strain is distributed inhomogeneously between the elastically loaded austenite (strain ~1%) and detwinned martensite (strain ~8%) [28–31]. Accordingly, the Strain-N fatigue curves reported on NiTi wires are inaccurate as they do not reflect the inhomogeneous nature of deformation. In addition, the strain localization has been found critical for the failure of NiTi wires cycled in transformation regime [32].

To sum up, the localization of transformation deformation in superelastic NiTi makes it impossible to use the experimental fatigue data measured on superelastic NiTi wires loaded in tension for evaluation of fatigue performance at the onset of martensitic transformation. We have tried to find a way around this. Additionally, we have tried to find out what is the role of the R-phase transformation in the fatigue of superelastic NiTi. The problem is that the transformation from cubic B2 austenite to trigonal R-phase transformation [3] usually precedes the martensitic transformation in medical graded NiTi wires [33,34] and obscures the fatigue experiments. The R-phase transformation is often neglected in fatigue studies as it is hard to be distinguished from the elasticity. B2-R transformation yields relatively small strains (~0.5%) compared to the strains due to B2-B1' martensitic transformation. But it is a true stress induced martensitic transformation as evidenced by latent heat or electric resistance changes. We believe it might play important role in fatigue tests near the onset of martensitic transformation as these strains are comparable to elastic strains in this regime.

We used special NiTi wire samples grinded and electropolished into an hourglass shape. Such samples were used in a pioneering fatigue work on NiTi by Melton and Mercier [9]. We found that the hourglass shape indeed confines transformation processes into a well-defined gauge volume and prevents the localization of deformation. The pull-pull S-N curves can be measured exactly within the requested range covering the fatigue life drop from million to few thousands of cycles. By selecting two different testing temperatures, the fatigue of NiTi was investigated for (i) B2 elasticity and for (ii) B2 elasticity combined with B2-R-phase transformation. Fracture surfaces of fatigue-failed samples were investigated using optical and scanning electron microscopy revealing five different stages of fatigue crack propagation. Finally, supplementary experiments using fast infrared thermography and force-displacement hysteresis measurements completed our experimental campaign motivated by the question of how the fatigue failure of superelastic NiTi is related to phase transformation processes.

## 2. Geometry and material

Analysis of the fatigue behavior of superelastic NiTi wires near the onset of stress-induced martensitic transformation is hindered

by the localization of the transformation [28–31], which is often prematurely initiated by clamping pressure in grips. The transformation localizes into martensite bands, making it impossible to measure the fatigue performance with respect to strain. Once the martensite band has been nucleated, the material in it deforms to large strains (~8%) through detwinning even if external strains are small (~1%). Therefore, to study the drop in fatigue performance of superelastic NiTi near the onset of the martensitic transformation regime, we used hourglass shaped samples shown in Fig. 1. Thanks to the hourglass shape, all fatigue and transformation processes are confined into the central volume of the sample. The hourglass shaped samples were produced from as drawn NiTi wires through grinding followed by electropolishing. Then, the samples were subjected to heat treatment. Note that the continuously changing cross-section makes the mechanical response different from the typical superelastic response of straight wires as discussed in detail in the next section.

Compared to wire diameters usually applied in medical devices, we selected a rather large wire diameter that could be processed into the hourglass shape. We selected a cold drawn 1.78 mm NiTi wire made by Fort Wayne Metals Ltd. (FWM) from medical graded alloy denoted NiTi#1 [35]. FWM certified the final cold work of

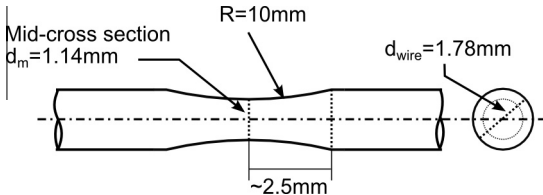


**Fig. 1.** Geometry of hourglass shaped samples.

~40% and nominal composition 50.92 at.% Ni. The 5 mm long hourglass shaped central volume of the sample is formed by a radius of 10 mm reducing the diameter continuously down to 1.14 mm at the mid-cross-section (Fig. 1). As-processed hourglass shaped samples were finally heat treated in an air furnace at 500 °C for 30 min and water quenched, resulting in recovery of cold drawn microstructure. Such heat treated samples show thermally induced transformations (see DSC curves in Fig. 2a) from which the functional behavior of NiTi is derived. Upon cooling, the samples undergo martensitic transformation from cubic B2 austenite to trigonal R-phase between temperatures  $R_s$ - $R_f$  and upon further cooling to monoclinic B19' martensite between temperatures  $M_s$ - $M_f$ . Upon heating, partly overlapped reverse transformations from martensite to R-phase and austenite take place between temperature  $R_s'$ - $A_f$ . All transformation temperatures, as identified from Digital Scanning Calorimetry (DSC) curve in Fig. 2a, are listed in Table 1.

Martensitic transformations can be also stress-induced when reaching associated critical stresses needed for individual transformations to proceed. As discussed in the next section, the stress-induced transformation into martensite can be detected at the peak of stress in the mechanical response of a deformation-controlled quasi-static tensile test (Fig. 2c). As tensile behavior of superelastic NiTi wires are strongly temperature dependent, we performed fatigue testing at two different temperatures 40 °C

**Table 1**  
Transformation temperatures as identified from DSC measurement.

T (°C)	$R_s$	$R_f$	$R_s'$	$A_f$	$M_s$	$M_f$
27	11	—	—1	35	—48	—105

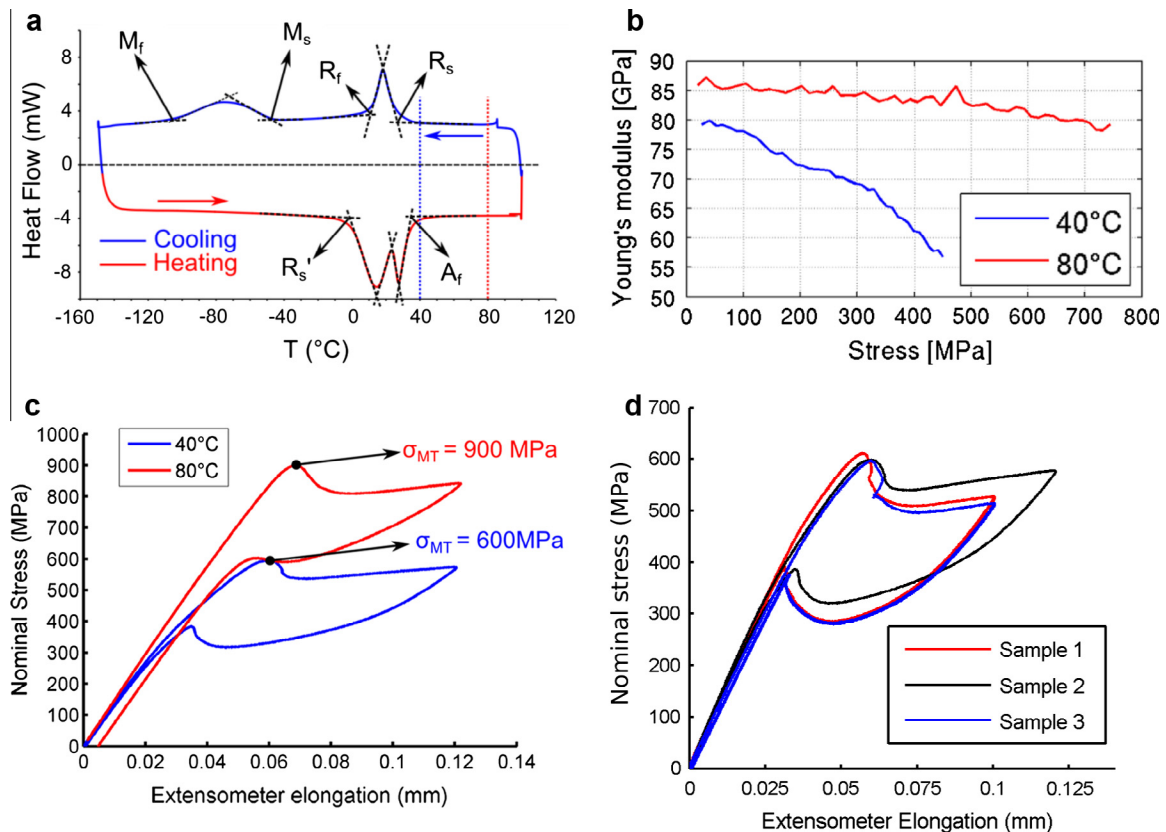


**Fig. 2.** Thermomechanical characterization of tested samples in terms of (a) phase transformation temperatures measured by DSC, (b) Young's modulus softening related to stress-induced R-phase transformation measured by DMA, (c) displacement controlled tensile responses, (d) tensile responses of three virgin samples at 40 °C.

and 80 °C. At 40 °C the critical stress for the onset of martensitic transformation is 595 MPa whereas at 80 °C it is 880 MPa in accord with Clausius–Clapeyron relation [3]. On the other hand, the stress-induced transformation from austenite to R-phase can be detected as a continuous softening of Young's modulus [36] at stresses below the martensitic transformation stress. The heat treated concave shape samples show an important Young's modulus softening at 40 °C, whereas at 80 °C the softening is negligible, as measured through a Dynamical Mechanical Analysis (DMA) analysis (Fig. 2b). In other words, the stress-induced R-phase transformation is well pronounced at 40 °C but not present at 80 °C.

### 3. Thermomechanical response of hourglass shaped samples

The hourglass shaped samples respond to tensile loading differently from straight wires. Therefore, we carefully analyzed the thermomechanical response of the hourglass shaped sample in order to correctly associate the stress amplitudes and temperatures of fatigue tests with local strains and operating deformation processes. We measured the deformation and temperature fields in the concave shaped zone during tensile loading by using 2D Digital Image Correlation (DIC) and fast infrared thermography, respectively. In this way we try to deal with the problems stemming from the inhomogeneous transformation and fatigue life driven by local strain values.

Unlike tensile responses of straight wires in position controlled tests showing a typical stress plateau related to forward and reverse martensitic transformation (Fig. 3b), hourglass shaped samples responses show a stress peak at the onset of martensitic transformation marked as loading stage 4 in Fig. 3b, beyond which the stress drops and further on increases monotonically again. However, the local material response in the mid-point of the sample shown in Fig. 3c resembles that of the straight wire showing a typical stress plateau associated with the deformation processes through the forward (loading) and reverse (unloading) martensitic

transformation. Contrarily to straight wires, the stress plateau of the local response possesses local minima. Moreover, the local response is nonlinear prior to the onset of martensitic transformation (loading stages 1–3), which indicates the inelastic deformation process through the transformation into R-phase as also indicated by thermography.

The local strain response was measured using 2D DIC – i.e. neglecting the out of plane displacements. DIC enabled to track in-situ surface strains during loading and unloading at room temperature (32.5 °C). From 2D strain fields we could track the strain profiles along the sample's axis (Fig. 3d) and, thus spatially resolve the transformation strains that exceed the elastic deformation of the austenite phase. At loading stage 4 the deformation is twice as large as the elastic deformation of austenite (considering Young's modulus of 86 GPa as measured by DMA). In other words, the martensitic transformation commences at stage 3 and proceeds homogeneously through the gauge volume up to stage 4 coming at an elevated strain rate (Fig. 3e). Further on, the strain rate decreases, transformation starts to spread out of the mid-point of the hourglass shaped zone, and local deformation grows up to more than 7% (loading stage 8). In [supplementary material, supplementary movie 1](#) summarizes the DIC analysis of hourglass sample's tensile response.

Furthermore, we used fast thermography to associate the appearance of deformation/transformation processes with nominal stresses and testing temperatures. The thermography takes advantage of latent heat exchange arising from forward and reverse phase transformations in superelastic NiTi [29]. In [supplementary material, supplementary Fig. 1](#) presents results of in-situ thermography during force-controlled tensile tests carried out at high strain rates intended to produce adiabatic conditions. There, we present thermomechanical evolutions in terms of nominal stresses in the mid-cross-section, temperatures averaged in the vicinity of the mid-point, and temperature profiles along the sample's axis within the hourglass shaped zone. The results clearly show that

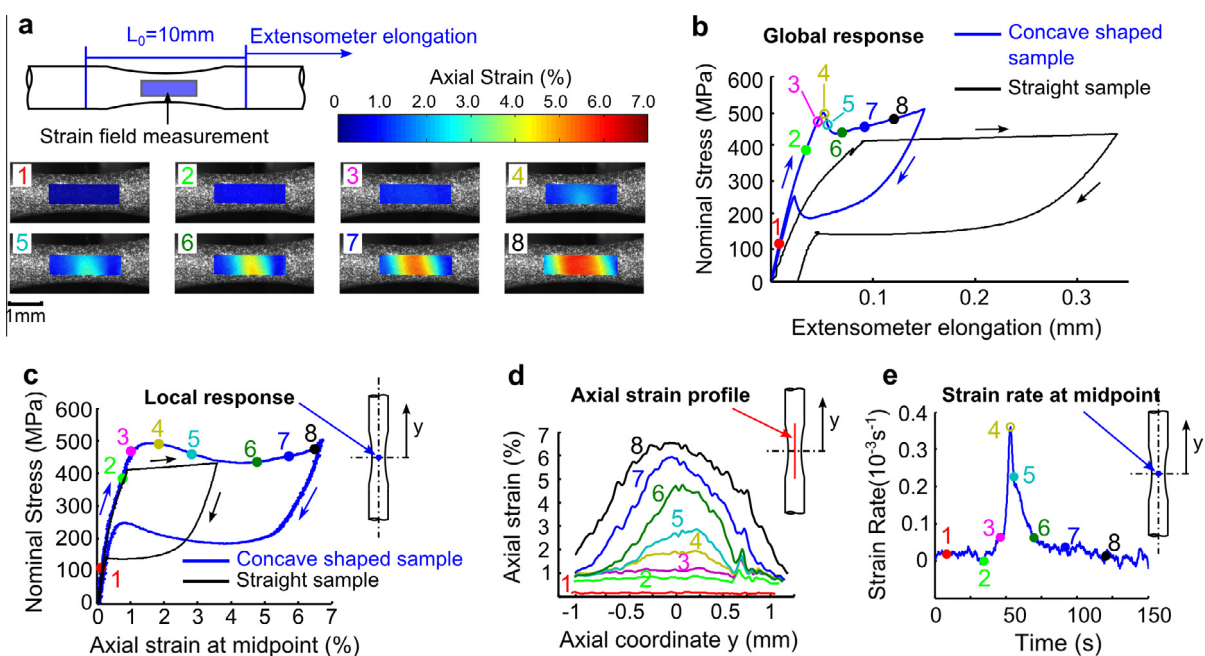


**Fig. 3.** Features of the hourglass sample's response to displacement controlled tensile loading ( $10^{-3}$  mm/s) at room temperature (32.5 °C). (a) Axial strain fields measured by DIC in the sample's hourglass zone experiencing the highest tensile stresses. (b) Comparison of tensile responses as measured by a clip-on extensometer on both the hourglass sample and the straight wire sample. The highlighted loading points correspond to the axial strain fields shown in (a). (c) Local superelastic response at the mid-point relating the nominal applied stresses to the mid-point axial strain obtained by averaging the axial strain field from DIC over a square area of  $13.7 \times 13.7 \mu\text{m}^2$ . (d) Evolution of axial strain profiles identified from axial strain fields in (a) for reference points denoted in global and local tensile responses (b) and (c). (e) Evolution of the axial strain rate at the mid-point identified from the time evolution of the mid-point axial strains.

the deformation through the R-phase transformation operates at the testing temperature of 40 °C when nominal stresses exceed 200 MPa as indicated by an increase in temperature due to a latent heat release. At 80 °C cooling upon loading due to thermoelastic effect prevails until the stress exceeds 590 MPa, then the temperature increases slightly before the martensitic transformation is triggered. This indicates that the R-phase transformation is only retarded and not fully suppressed at 80 °C. As for the martensitic transformation, it appears clearly at both testing temperatures, 40 °C and 80 °C, beyond nominal stresses of 600 MPa and 900 MPa, respectively, as evidenced by a sharp temperature increase.

To sum up, the experimental observations showed that unlike in straight wires the transformation processes are effectively confined into the hourglass shaped zone and strains linked to these processes evolve continuously upon straining. Moreover, the selected heat treatment sets transformation temperatures so that the R-phase transformation proceeds earlier at 40 °C while it is retarded at 80 °C.

#### 4. Results of fatigue testing: stress-strain-N curves

The hourglass shaped samples were subjected to pull-pull fatigue cycling in the force-controlled regime at temperatures 40 °C and 80 °C while the deformation was measured by a dynamic clip-on extensometer with 10 mm gauge length attached to the sample as shown in Fig. 3a. The runout of the fatigue testing was set to 1.5 million cycles. Applied nominal stress amplitudes involved deformations through elasticity, R-phase transformation and martensitic transformation. Note that the effect of the temperature change is twofold. First, it affects the R-phase transformation being almost suppressed at 80 °C while well pronounced at 40 °C. Therefore, testing at 40 °C emphasized the deformation through the R-phase transformation involved in most applied amplitudes while testing at 80 °C emphasized the elastic deformation of austenite at amplitudes below the onset of martensitic transformation. Second, the temperature changes the critical stress for the onset of martensitic transformation ( $\sigma_{MT}$ ). At 80 °C, the onset appears at 900 MPa while for 40 °C it appears at 600 MPa.

Surprisingly, the runout at 80 °C was reached at 543 MPa being 139 MPa higher compared to the value reached at 40 °C (404 MPa) as clearly seen in the Stress-N curves identified at both the temperatures in Fig. 4. Above the runout stresses ( $S_r$ ), both S-N curves present a continuous reduction of the number of cycles to failure being a transition towards the low cycle fatigue regime (LCF).

In an attempt to provide a tool for prediction of the fatigue performance of superelastic NiTi, namely the transition towards LCF, we hereby suggest a simple model which is able to take into account the temperature dependence of the fatigue behavior as

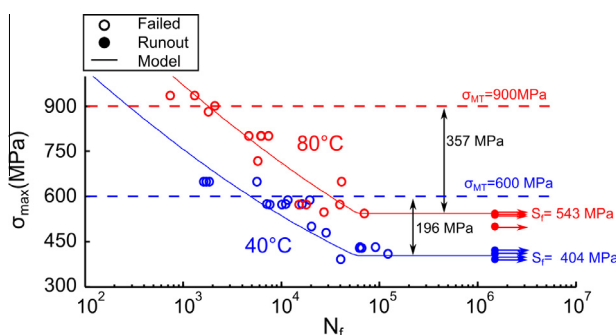


**Fig. 4.** Stress-N curves in terms of peak of nominal stresses at mid-cross-section of hourglass shaped samples plotted from results of force controlled pull-pull fatigue tests performed at 40 and 80 °C, R ratio of 0.1 and frequency of 25 Hz.

observed experimentally. The model is based on the Basquin's power law relation [37] as the transition towards LCF presents linear trend in the logarithmic scale. Since the experiments show an increase in fatigue life limit with temperature we embedded linear temperature dependency into our model suggesting the relation between the equivalent stress  $\sigma_{eq}$  and the number of reversals 2  $N_f$  as follows:

$$\sigma_{eq} = \gamma \sigma_u (T - M_s) (2N_f)^b \quad (1)$$

where  $\sigma_u$  relates the fatigue limit to the ultimate tensile strength, while the temperature dependence of the fatigue limit is implemented through a fatigue strength temperature sensitivity parameter,  $\gamma$ , testing temperature,  $T$ , and temperature,  $M_s$  of the transformation towards martensite upon cooling in unloaded state as identified from DSC measurement (Fig. 2, Table 1). The rate of the transition towards LCF is expressed by fatigue strength exponent,  $b$ . The linear temperature dependence of the fatigue limit is based on the assumption that the fatigue limit is also related to the critical stress for the onset of martensitic transformation, which scales linearly with the temperature difference from  $M_s$ . We consider the equivalent stress  $\sigma_{eq}$  taking into account the relation among the stress amplitude,  $\sigma_a$ , mean stress,  $\sigma_m$ , and ultimate tensile strength,  $\sigma_u$  according to the Goodman model as follows:

$$\frac{\sigma_a - \sigma_m}{\sigma_{eq} - \sigma_u} = 1 \quad (2)$$

Fitting parameters  $\gamma$  and  $b$  are listed in Table 2 along with the material parameters. Fitting parameters were identified by least square method using results of fatigue tests performed at 40 °C. As seen in Fig. 5, the model predicts well the temperature sensitive transition towards the LCF when approaching the onset of martensitic transformation. Nevertheless further experimental verification of the model is required to evaluate its general applicability to superelastic NiTi. Notably, a possible relation of fatigue strength temperature sensitivity parameter  $\gamma$ , being now a fitting parameter, to the temperature dependence of the critical stress for the onset of martensitic transformation, being a material parameter, is to be investigated.

Beside the stresses, large transformation strains that do not scale with stresses play an important role in fatigue of SMAs [4–6]. Therefore, we constructed a Stress-Strain-N graph showing how the number of cycles to rupture evolves with both the peaks of maximum nominal stresses and the peaks of local strains in the mid-point evaluated from stabilized cycles (see Fig. 5).

The way of obtaining the peak of local strains, however, is not straight forward. It was calculated as a sum of the local elastic deformation of austenite ( $E \sim 86$  GPa see Fig. 2b) and local transformation deformation deduced from the elongation of the clip-on extensometer as follows. The total local deformation was first measured by DIC together with the extensometer elongation at room temperature (see Fig. 3). Then, subtracting the elastic deformation, relation between the local transformation deformation and the extensometer elongation could be plotted as shown in Fig. 5b. Note that we assume this relation to be independent of temperature.

**Table 2**

Material and fitting parameters of suggested fatigue prediction model (Eq. (1)) as measured and identified on studied superelastic NiTi. Fitting parameters were identified by least square method using results of fatigue tests performed at 40 °C.

Material parameters		Fitting parameters	
Ultimate tensile strength $\sigma_u$ [MPa]	Transformation temperature $M_s$ [°C]	Fatigue strength exponent $b$ [-]	Fatigue strength temperature sensitivity $\gamma$ [1/°C]
1400	-48	-0.2	0.02

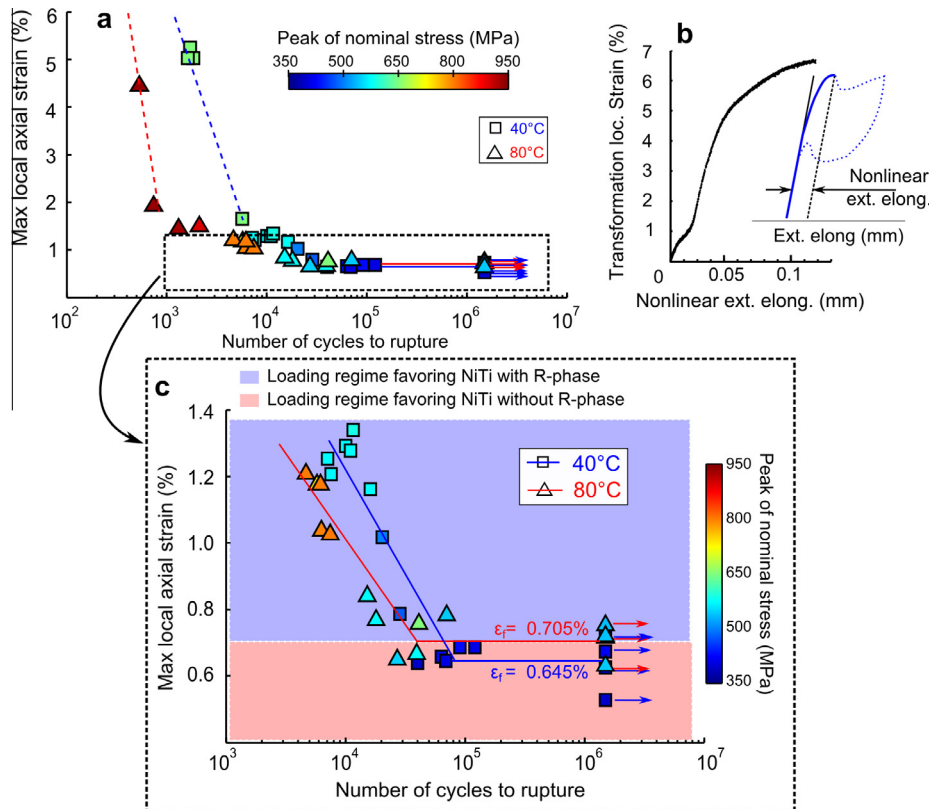


**Fig. 5.** Stress-Strain-N graph resulting from pull-pull fatigue testing with R ratio of 0.1 performed in force controlled regime at temperatures of 40 °C and 80 °C. (a) Stress-Strain-N graph shows the fatigue life versus peak of nominal stresses and corresponding maximum local strains identified from stabilized stage of fatigue cycling. For better visualization of the transition from millions cycles to a few thousands, highlighted area is shown in (c). The maximum local strains were deduced from experimentally identified dependence of the local transformation strain (from DIC) on extensometer elongation (b).

Thanks to this relation, it was possible to identify the peak of local strain for any stabilized peak of extensometer elongation measured during a fatigue test. As it will be discussed later, the peak of extensometer elongation was stable over the complete fatigue test duration with exception of few tens of cycles before rupture. Therefore, we can consider this peak as a representative value of the strain to which the sample is subjected during the fatigue test.

Unlike Stress-N curves in Fig. 4, Stress-Strain-N graph in Fig. 5a shows the fatigue curve in terms of strains while stresses are represented by markers' colors<sup>1</sup>. The Stress-N curves clearly promote elastically deforming NiTi at 80 °C as a best fatigue performer within the entire range of applied loadings. However, in the strain representation, NiTi cycled at 80 °C outperforms NiTi at 40 °C within a limited range of applied loadings where strains stay below 0.7% (red zone in Fig. 5c). Beyond 0.7% (blue zone in Fig. 5c), the elastically deforming NiTi develops much larger stresses compared to NiTi where the R-phase transformation acts as a stress reliever.

From Stress-N and Stress-Strain-N graphs in Figs. 4 and 5 we further notice that the fatigue performance of superelastic NiTi at temperatures of 40 °C and 80 °C drops down from 10<sup>6</sup> to few 10<sup>4</sup> cycles at 404 MPa and 543 MPa, respectively. These values are respectively 196 MPa and 357 MPa below the critical stresses needed for martensitic transformation to proceed being 600 MPa and 900 MPa, respectively. Approaching and finally reaching these critical stresses lead to a continuous but not accelerated worsening of fatigue performance. Furthermore, the drop in fatigue performance is not associated with large martensitic transformation strains typical to superelastic use of NiTi (recoverable strains up

to 10%). The dramatic drop in fatigue performance of superelastic NiTi appears at strains dominated by elastic deformation or inelastic deformation through the R-phase transformation.

Based on distinct conclusions drawn from both Stress-N and Strain-N representations, we believe that Stress-Strain-N graph carrying information on both the strains and the stresses is the only relevant fatigue life representation for SMAs. Unfortunately, it can be meaningfully used only in conjunction with specimens that don't display strain localization and continuous strain dependence on loading is guaranteed within the gauge volume.

## 5. Fatigue crack characterization

We analyzed the morphology and size of fatigue cracks in order to better understand the fatigue failure and fatigue crack propagation in superelastic NiTi wires. We thoroughly examined the fatigue crack surfaces using 3D optical microscope and SEM. Consequently, we were able to draw a picture of a typical fatigue crack surface of superelastic NiTi wires loaded near the martensitic transformation regime. The picture (Fig. 6) distinguishes five zones with distinct morphologies on the fatigue crack surface (unlike three zones described in [18]). The river marks, well visible in 3D optical microscope, point to the crack initiation zone (Fig. 6 1.S<sub>in</sub>) with morphology affected by surface rubbing and pounding. This zone merges into the second zone having quasi-cleavage morphology (Fig. 6 2.S<sub>cl</sub>). The quasi-cleavage zone disappears into the third zone of fatigue striations (Fig. 6 3.S<sub>st</sub>) from which the fourth zone of mixed mode between striations and ductile fatigue crack surface with dimples emerges (Fig. 6 4.S<sub>df</sub>). Finally, ductile overload surface is again well noticeable on 3D light microscope image

<sup>1</sup> For interpretation of color in Fig. 5, the reader is referred to the web version of this article.

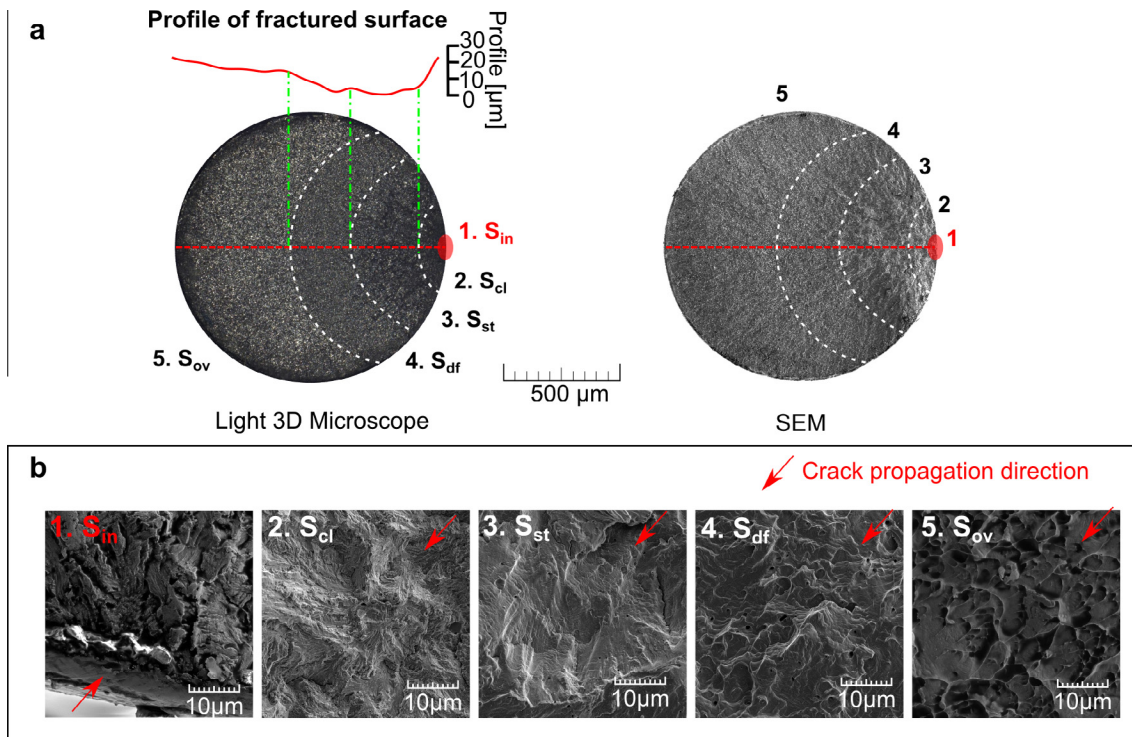


**Fig. 6.** (a) Typical fatigue fracture surface as viewed from light 3D microscope and SEM. (b) Five zones with distinct morphology were identified on the fracture surface. River marks point to fracture initiation zone 1 that is followed by zone 2 with quasi-cleavage morphology continued with fatigue striation zone 3, ductile fatigue crack zone 4, and ductile overload zone 5.

(Fig. 6 1.S<sub>ov</sub>). This characteristic picture of the fatigue crack surface is preserved for nominal loadings involving stress-induced martensitic transformations, however, the size of zones 4 is in this case reduced as discussed below.

More detailed SEM micrographs of fatigue crack surfaces are presented in [supplementary material](#). Matrix of SEM micrographs presented in [supplementary Fig. 2](#) shows the morphology of zone 2 as it changes with temperature and peak of nominal stress. Matrix of SEM micrographs presented in [supplementary Fig. 3](#) shows the morphology of fatigue striation zone 3 as it changes with temperature and peak of nominal stress.

Size analysis of the fatigue crack surfaces revealed that the fatigue crack area scales inversely with the peak of nominal stress (Fig. 7a and b) while it is proportional to number of cycles to failure (Fig. 8). When the fatigue loading is near the runout limit the total crack area reaches almost 50% while for fatigue loadings near the martensitic transformation regime the total crack size drops down to 10%. In addition when nominal fatigue loadings involve martensitic transformation, the crack initiation, quasi-cleavage and fatigue striation zones occupy in total less than 5% of the initial cross-section (blue curve in Fig. 8). Therefore, the quasi-cleavage zone of the crack may be often omitted in analysis of fatigue cracks of NiTi wires cycled in the martensitic transformation regime [18].

We evaluated the normal stresses at the final overload taking into account measured tensile force and reduced cross-section. As seen in Fig. 9, the normal stresses scatter around a constant average value for a given testing temperature and all applied loadings. The average normal stress for the testing temperature of 80 °C (1000 MPa) was substantially higher compared to 40 °C (750 MPa). For all tests, however, the normal stress acting at final failure on the cross-section reduced by the crack size exceeds the value  $\sigma_{MT}$  of the critical stress for the onset of martensitic transformation (see Fig. 9).

## 6. Discussion

The performed fatigue tests revealed that the fatigue performance of NiTi is highly reduced from  $10^6$  to  $10^4$  cycles even before the nominal fatigue loadings reach the martensitic transformation regime and related high strains. However, analysis of fatigue crack surfaces showed that the normal stress acting in the reduced fatigue overloaded cross-section is well above the stress needed to induce the martensitic transformation. It suggests that the fatigue cycling in elastic or R-phase transformation regimes switches into the martensitic transformation regime once the crack reaches a critical size. Note that we disregard the complex stress concentrations at the crack tip where localized martensitic transformation may be triggered before the normal stress reaches the critical value. Nevertheless, to verify this scenario we performed dedicated experiments focused on the evolution of hysteresis, crack opening and temperature changes within the gauge volume. The fast thermography during complete fatigue tests indeed revealed that the fatigue damage triggers local transformation processes in about 60% of fatigue life and that the final failure is accompanied by inhomogeneously proceeding transformation processes. Moreover, the transformation deformation proved to assist the crack growth as it enlarges the crack opening.

The transition towards martensitic transformation regime is noticeable by tracking the evolution of force-displacement hysteresis during the tensile test. As seen in Figs. 10 and 11a the hysteresis starts to progressively increase few tens of cycles before the rupture, which is due to increasing deformation as the fatigue tests are force controlled. Specifically, the deformation increases beyond the limits of elastic and R-phase transformation in an unstable manner so that the tensile machine is unable to control the force amplitude which actually drops while the displacement amplitude keeps increasing as shown in Fig. 10. The increase in hysteresis is more pronounced for nominal fatigue loadings in R-phase or

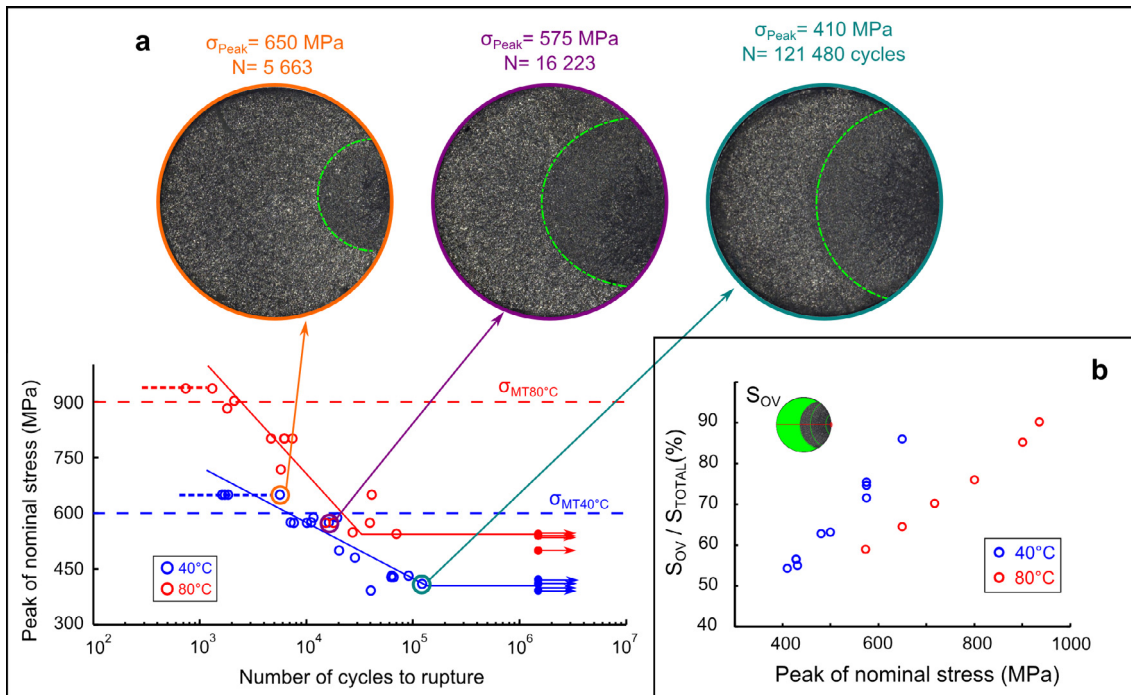


**Fig. 7.** Size dependence of fatigue crack surfaces on the peak of nominal stress for two testing temperatures 40 °C and 80 °C. (a) Fracture surface with denoted final overload surfaces for samples subjected to three different peaks of nominal stress. (b) Dependence of the relative size of overload surfaces on the peak of nominal stress.

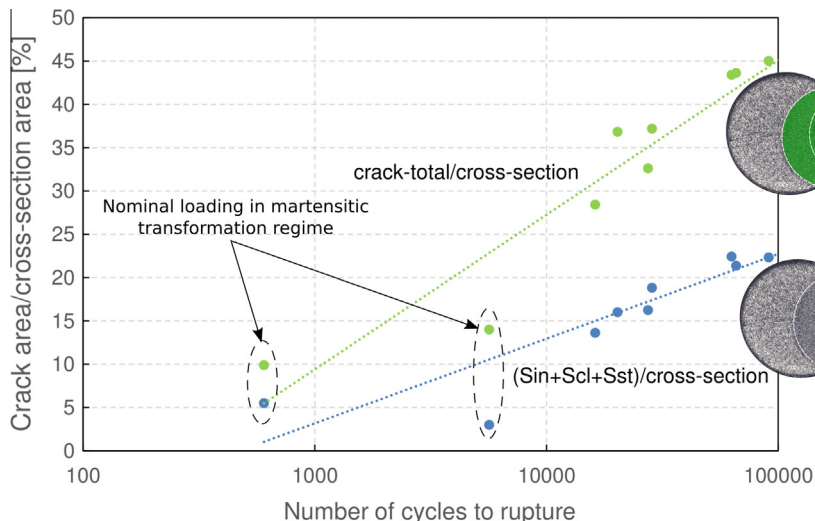


**Fig. 8.** Evolutions of crack surface areas with number of cycles to rupture identified for fatigue testing temperature of 40 °C. The total crack area is plotted in green. A part of the crack area including crack initiation, quasi-cleavage and fatigue striation zones is plotted in blue. (For interpretation of the references to color in this figure legend, the reader is referred to the web version of this article.)

martensitic transformation regimes compared to the elastic regime at 80 °C as illustrated in Fig. 11a, b.

The uncontrolled increase in the hysteresis indicates an uncontrolled crack growth. To verify this we arrested a fatigue test at the onset of the hysteresis increase (Fig. 12a). The arrested test was performed at 40 °C, 25 Hz,  $R = 0.1$  and peak of nominal stress of 580 MPa being below the stress inducing the martensitic transformation. After the arrest, the sample was tensile loaded till rupture at room temperature (32 °C) while measuring the crack opening and local strains near the crack using DIC (Fig. 13). The fracture surface was then compared to the fracture surface of a sample cycled under the same conditions till the final fatigue failure

(Fig. 12b). When comparing their respective fatigue surfaces, the fatigue crack penetration depth from the arrested test was only 81 µm shorter and the crack surface was 7% smaller, evidencing the advanced stage of fatigue crack propagation at which the test was arrested. At this stage, the maximum normal stress in the reduced cross-section is high enough to induce the martensitic transformation and related strains. Measurements of local strains near the crack (Fig. 13) revealed the critical effect of the transformation strain to the crack opening. In fact, the crack opening is enhanced by large strains ahead of the crack caused apparently by stress induced martensitic transformation. For simplified interpretation, let us assume local tensile deformations up to 7% that

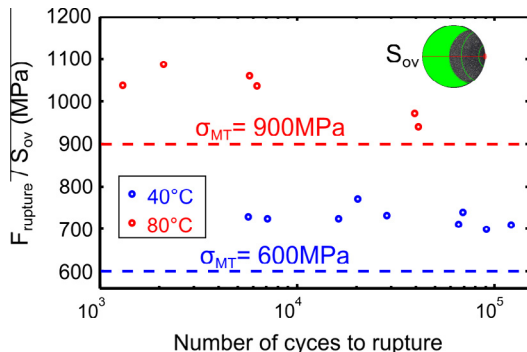


**Fig. 9.** Normal stresses at the final overload evaluated for both testing temperatures of 80 °C and 40 °C as a ratio between the force at fatigue rupture and the overload surface identified from microscopy.

can be reversibly stress-induced by martensitic transformation when the critical stress for its onset is reached as identified on a virgin wire sample (Fig. 3c) and hourglass sample (Fig. 5b). This deformation appears gradually from the stress concentrating crack tip towards the rest of the reduced cross-section as illustrated in Fig. 13a and b by loading stages A-D where local strains were measured by three virtual extensometers using DIC. Gradual spread of the tensile transformation deformation within the reduced cross-section enhances the crack opening (Fig. 13c) that results in large local strains at the crack tip reaching up to 25% in stage D (Fig. 13b). Such large deformation is by far beyond the reversible strains accommodated at moderate plateau stresses by martensitic transformation, and, hence, large stresses must arise at the crack tip. Indeed, the rupture occurred immediately when the large strain of 25% at the crack tip had been reached. To sum up, stress-induced martensitic transformation strains assist the crack

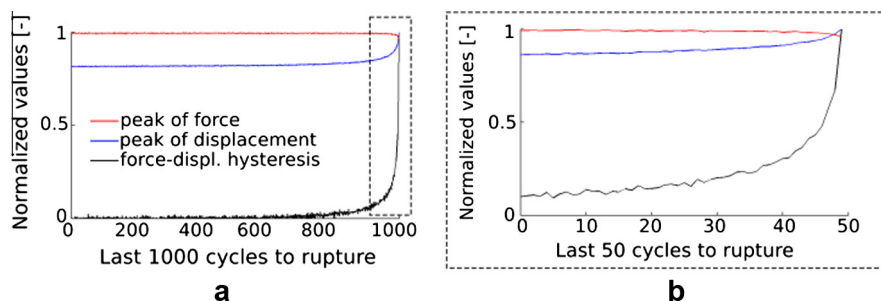


**Fig. 10.** The evolution of fatigue loading in terms of peaks of force and extensometer displacement, and force-displacement hysteresis in last 1000 cycles before failure (a) with a zoom to last 50 cycles (b) where the loading conditions evolves with the highest rate. The results correspond to fatigue cycling at 40 °C with peak of nominal stress of 430 MPa.

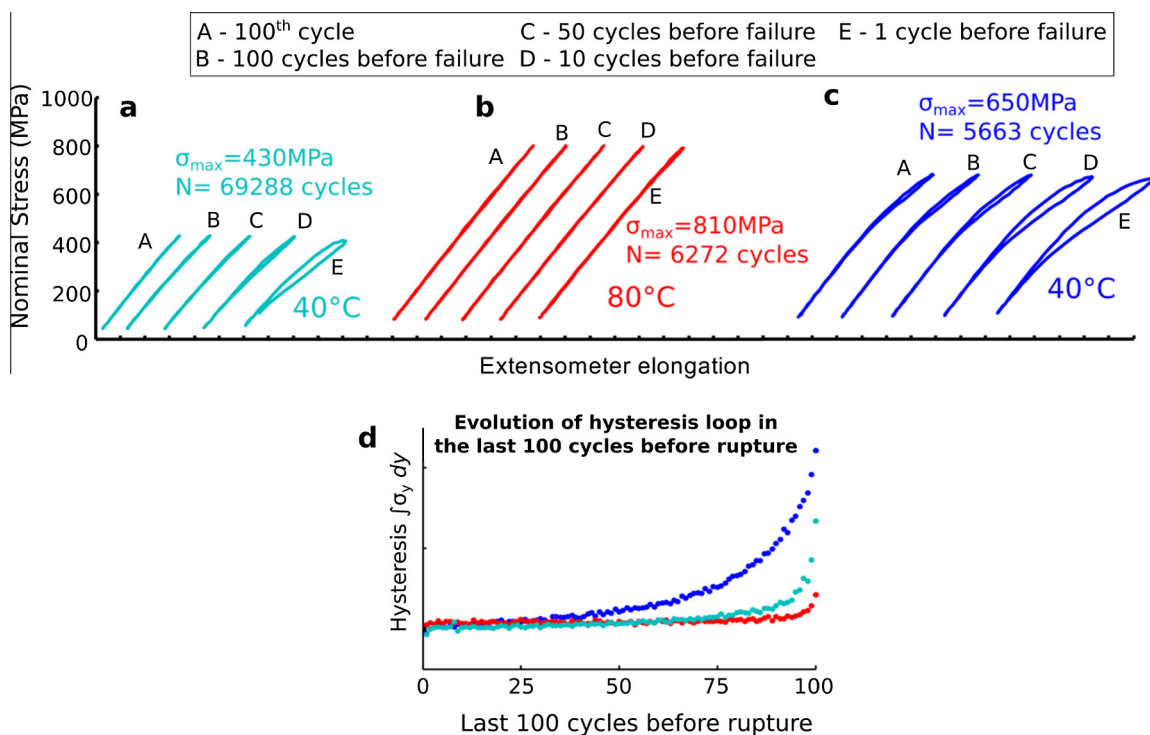


**Fig. 11.** Evolution of tensile responses of hourglass shaped samples over 100 cycles before failure during fatigue cycling in force controlled regime with peaks of nominal stresses below the martensitic transformation regime at (a) 40 °C, (b) 80 °C, and (c) within the martensitic transformation regime at 40 °C. Related evolutions of force-displacement hysteresis are shown in (d). Note that the cyclic responses and hysteresis do not change over cycling until few tens of cycles before fatigue failure.

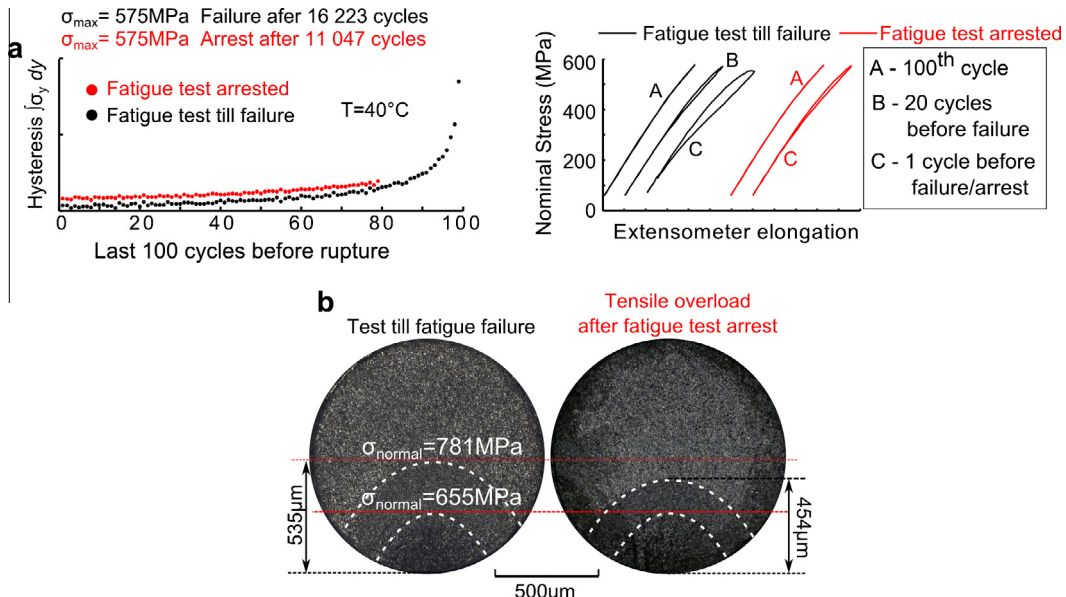


**Fig. 12.** Observations of fatigue damage of an hourglass sample prior to fatigue failure at the onset of hysteresis increase upon which the fatigue test was arrested (a). The arrested fatigue test was performed at  $40^\circ\text{C}$  with R ration of 0.1, peak of nominal stress at 580 MPa being below the nominal stress for martensitic transformation. (b) A large crack was located on the sample and its opening was measured upon quasistatic tensile overloading at room temperature ( $32^\circ\text{C}$ ).

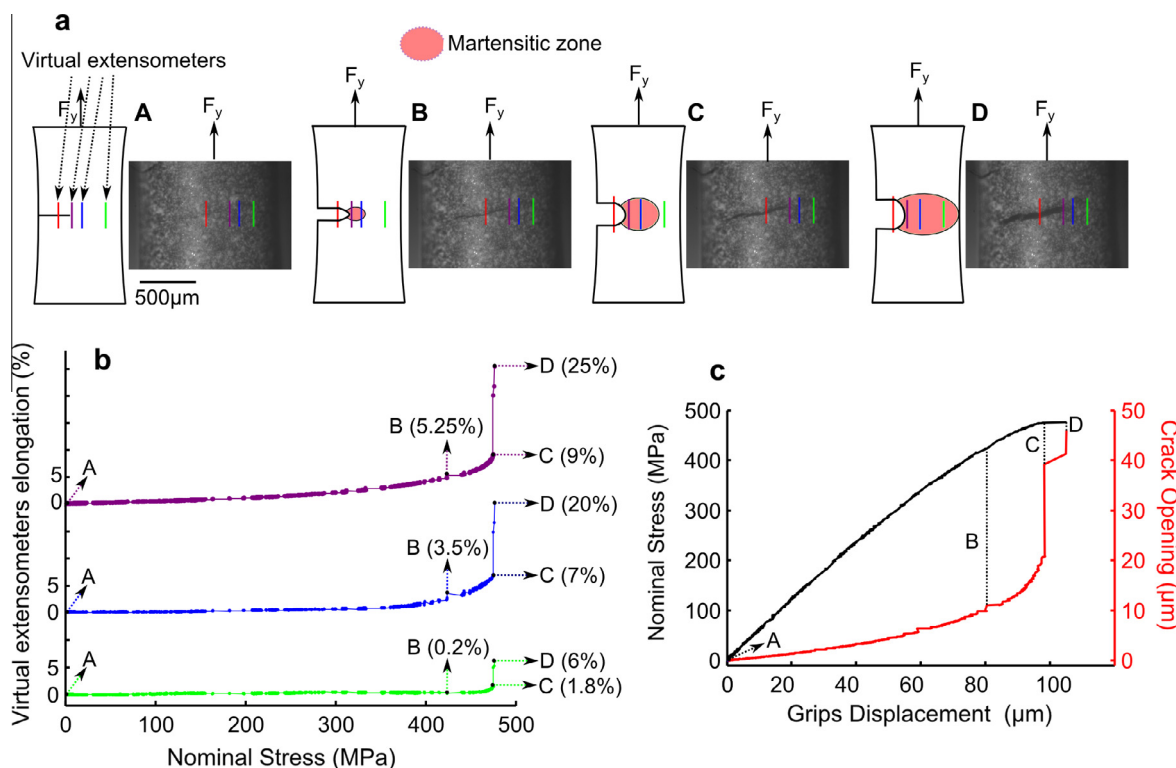


**Fig. 13.** The crack opening and local strains near the crack tip as measured on the sample after a fatigue test arrest prior to failure as described in Fig. 12. The measurement was performed during a force controlled tensile test till failure. Spread of martensitically transforming zone illustrated in (a) is based on three virtual extensometers' elongation measurements near the crack tip (b) and on the crack opening measurement (c) all realized using DIC method.

opening leading to high crack tip strains and, presumably, to high stresses thus promoting the crack growth.

To further inspect the course of fatigue damage, we took advantage of the latent heat exchange due to R-phase and martensitic transformations to search for fatigue damage locally triggering these transformations. Therefore, we performed fast thermography

during complete fatigue tests at two applied temperatures. Note that for limited RAM capacity we could not perform the fatigue testing continuously but in several slots each containing about 2000 cycles. The fatigue tests were performed with nominal loadings below the martensitic transformation regime expecting appearances of localized heat sources and sinks related to phase

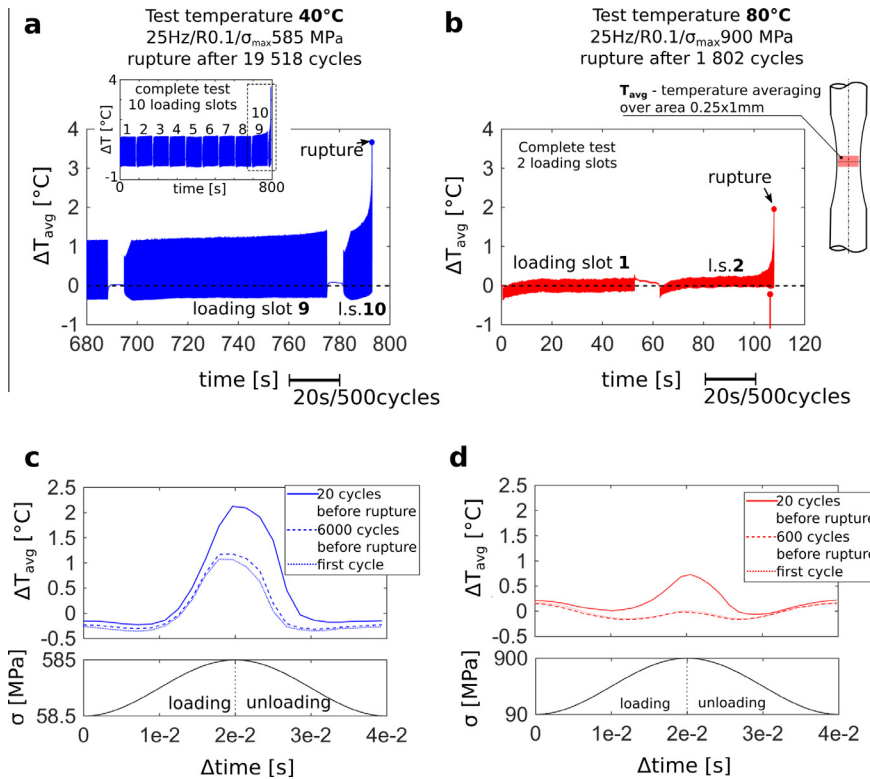


**Fig. 14.** Evolutions of temperature averaged over the gauge volume as recorded by IR camera during two fatigue tests performed for limited RAM in several interrupted slots; the first test lasting  $\sim 20e3$  cycles was performed at  $40^{\circ}\text{C}$ ,  $R = 0.1$ , 25 Hz, peak of nominal stress 585 MPa; the second test lasting  $\sim 2e3$  cycles was performed at  $80^{\circ}\text{C}$ ,  $R = 0.1$ , 25 Hz, peak of nominal stress 900 MPa. Graphs (a) and (b) show temperature evolutions during complete tests at  $40^{\circ}\text{C}$  and  $80^{\circ}\text{C}$ , respectively. Graphs (c) and (d) show one cycle temperature and stress evolutions in selected cycles of tests at  $40^{\circ}\text{C}$  and  $80^{\circ}\text{C}$ , respectively.

transforming zones triggered by stress concentrations at crack tips [38]. The test at  $40^{\circ}\text{C}$  was performed with peak of nominal stress 565 MPa; the failure occurred after about 20,000 cycles. The test at  $80^{\circ}\text{C}$  was performed with peak of nominal stress 900 MPa; the failure occurred after about 1800 cycles. First, we evaluated time evolutions of temperature averaged over the gauge volume as shown in Fig. 14a and b. The averaged temperature evolves within a cycle and over cycling as shown by selected one cycle evolutions in Fig. 14c and d.

For understanding single cycle temperature evolutions, one has to consider simultaneous actions of the thermoelastic effect and latent heat exchange due to both the R-phase and martensitic transformations, the actions of which are opposite. While the thermoelasticity cools down the sample upon loading and heats up the sample upon unloading, martensitic transformation heats up the sample upon loading due to latent heat release and cools down the sample by latent heat absorption upon unloading. Furthermore, large transformation enthalpies make the heat effects of transformations higher by orders of magnitude compared to thermoelasticity [39].

With previous paragraph in mind, one can see in Fig. 14c and d, that the extent of R-phase transformation, i.e. heating/cooling upon loading/unloading, is higher at  $40^{\circ}\text{C}$  than at  $80^{\circ}\text{C}$ . Moreover, as seen in Fig. 14a and b, the temperature maxima start rising in the final stage of fatigue life with a noticeably earlier onset of the increase for the test at  $40^{\circ}\text{C}$  similarly to the onset of the hysteresis increase (Fig. 11d). However, unlike hysteresis rising few tens of cycles before rupture, the temperature maxima start rising earlier – few hundreds of cycles before the failure.

Besides spatial temperature averaging, thermograms may reveal local heat effects (sources and sinks) that in the case of phase transforming NiTi may be related to localized damage acting as a stress riser thus triggering transformations locally [38]. How-

ever, transformations triggered by nominal loadings give rise to noticeable periodic temperature changes as seen in Fig. 14c and d that hide weaker local heat effects. Therefore, we evaluated so called differential thermograms that present temperature changes with respect to the temperature variations observed on a non-damaged sample subjected to fatigue cycling. Specifically, a differential thermogram for a given fatigue cycle and phase is computed from the related thermogram by subtracting the thermogram taken in the first fatigue cycle and given phase. Moreover, moving average was applied over few tens of cycles to filter out random noise allowing to reveal weak local heat effects giving rise to temperature changes smaller than  $0.1^{\circ}\text{C}$ . Using this technique, we were able to capture first periodic appearances of localized heat sources and sinks at approximately 60% of fatigue life i.e. 6000 cycle before rupture for the test at  $40^{\circ}\text{C}$  (Fig. 15a) and 600 cycle before rupture for the test at  $80^{\circ}\text{C}$  (Fig. 15b). In the case of the test at  $40^{\circ}\text{C}$  a second localized heat effect appeared 3000 cycles before rupture as seen in Fig. 15a and in [supplementary movie 2](#). With further cycling localized heat sources and sinks developed and grew to finally become well visible large localized heat effects few tens of cycles before rupture as illustrated in Fig. 15c and d and in [supplementary movie 3](#) showing that temperature changes reached up to few degrees. Note, that in the case of the test at  $40^{\circ}\text{C}$  the secondly appeared heat effect was the faster growing one that caused the final failure. The heat effects were more pronounced for the test at  $40^{\circ}\text{C}$  likely due to higher number of cycles to rupture (20,000 vs. 1800) and, hence, larger crack size (Fig. 8) allowing for larger crack openings.

We attribute the appearance of localized periodic heat effects with progressive intensity to martensitic transformation triggered by stress concentration along a tip of a well-developed steadily growing crack i.e. zone 3 of the fatigue crack marked with fatigue striations (Fig. 6). In fact, in such a state of fatigue damage, a

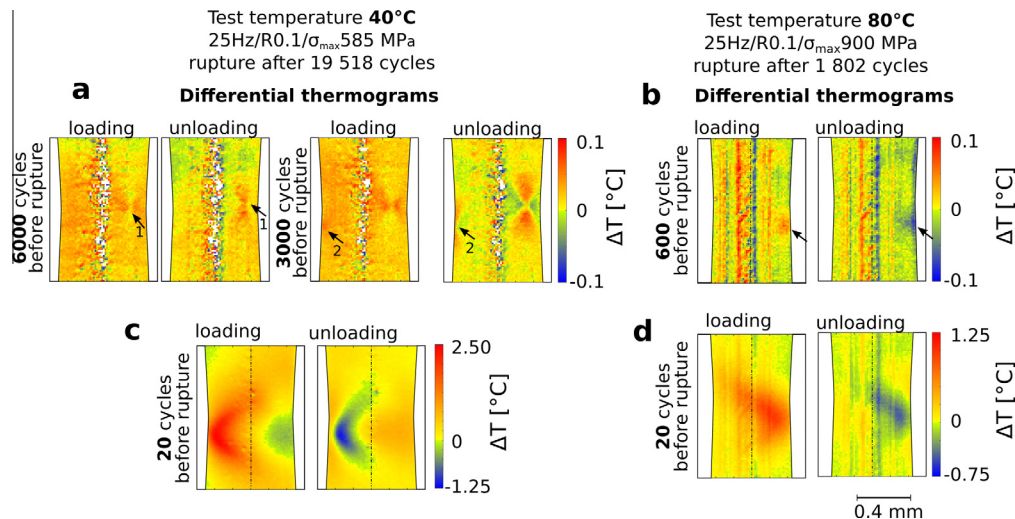


**Fig. 15.** Differential thermograms that evaluates spatially temperature changes with respect to virgin state recorded in the first fatigue cycle. Thermograms show temperature changes within the gauge volumes of hourglass samples at different cycles of two fatigue tests; the first test lasting ~20e3 cycles was performed at 40 °C, R = 0.1, 25 Hz, peak of nominal stress 585 MPa; the second test lasting ~2e3 cycles was performed at 80 °C, R = 0.1, 25 Hz, peak of nominal stress 900 MPa. Thermograms (a) show two localized heat sources and sinks as first spotted 6000 and 3000 cycles before rupture during the test at 40 °C. Thermograms (b) show localized heat source and sink as first spotted 600 cycles before rupture during the test at 80 °C. Thermograms (c) and (d) show localized heat sources and sinks 20 cycles before rupture of both the tests.

macroscopic volume of material is likely to experience stress concentration triggering the martensitic transformation thus inducing detectable temperature changes that appear periodically along with the applied loading. Nevertheless, for a more detailed interpretation of observed heat effects numerical modeling of heat effects is required.

To sum up, the fatigue performance of superelastic NiTi is largely affected by transformation processes and related deformations. The fatigue behavior of NiTi responds to transformation processes that operate nominally from first cycles or are triggered in NiTi when the crack size reaches a critical value. Therefore, nominal stresses and strains alone do not solely determine the fatigue performance of NiTi. Hence, any fatigue prediction model for NiTi must incorporate thermomechanical parameters governing constitutive behavior of NiTi and transformation processes proceeding in NiTi out of which most importantly the operating temperature, and transformation temperatures and stresses mutually bound through the Clausius–Clapeyron relation.

## 7. Conclusions

Fatigue performance of superelastic NiTi wires processed into hourglass shaped specimens was investigated to analyze the effect of deformation processes in stress controlled pull-pull fatigue tests with R = 0.1 and runout limit set to 1.5e6 cycles. Deformation processes including elasticity, stress-induced B2-R and B2-B1' transformations were assigned to individual test amplitudes and temperatures using thermography and DIC methods. The main experimental data are summarized in Stress-Strain-N fatigue curves for NiTi tested at 40 °C and 80 °C. At the lower testing temperature, the R-phase transformation preceded the martensitic transformation triggered at 600 MPa while at higher temperature elastic deformation of austenite preceded the martensitic transformation triggered at 900 MPa. Based on Stress-N curves, a model for prediction of temperature dependent fatigue behavior of superelastic NiTi was proposed. Furthermore, fracture surfaces were analyzed to come up with five zones of distinct fracture morphologies related to the degree of the fatigue fracture advancement.

It was found that fatigue performance of superelastic NiTi wires at 40 °C and 80 °C drops down from millions to thousands of cycles

at stress of 400 MPa and 540 MPa, respectively, being well below the stresses inducing the martensitic transformation being 600 MPa and 900 MPa, respectively. Moreover, the fatigue limits were reached at low strains of 0.65% (40 °C) and 0.7% (80 °C). It suggests that high strains related to martensitic transformation are not necessarily responsible for fast crack nucleation and early crack growth reported in superelastic NiTi. The R-phase transformation, on the one hand, proved to prolong the low cycle fatigue as it acts as a stress reliever reducing largely the stresses at higher strains above 0.7%. On the other hand, the martensitic transformation proved to assist the crack growth when its critical size has been reached. In fact, when the critical crack size has been reached the strains due to martensitic transformation provide additional driving force for the crack opening. Unfortunately, the critical crack size is reached sooner when nominal loadings are closer to the plateau stress i.e. the critical stress for the onset of martensitic transformation. Nevertheless, our results preserve the hope for high cycle superelasticity that might be possible if plateau stresses for martensitic transformation are lowered down below the structural fatigue limits inducing early crack nucleation and growth.

Conclusions drawn from different aspects of our experimental work are summarized as follows.

### Stress-Strain-N fatigue curves

- The runout limits (1.5e6 cycles) in terms of the peak of nominal stress were reached at 400 MPa and 540 MPa for NiTi exhibiting R-phase transformation and NiTi with retarded R-phase transformation, respectively.
- The runout limits (1.5e6 cycles) in terms of the peak of nominal stress were reached at 200 MPa and 360 MPa below the critical stress for the onset of martensitic transformation for NiTi exhibiting R-phase transformation and NiTi with retarded R-phase transformation, respectively.
- The runout limits (1.5e6 cycles) in terms of the peak of stabilized strain were reached at 0.65% and 0.7% for NiTi exhibiting R-phase transformation and NiTi with retarded R-phase transformation, respectively.
- The fatigue life drops down to 10<sup>4</sup> before the peak of nominal stress reaches the critical value for the onset of martensitic transformation.

- The fatigue life drops down to  $10^4$  before the peak of stabilized strains reaches 1%.
- The fatigue life drops from  $10^4$  to  $10^3$  when the peak of nominal stress enters the regime of martensitic transformation.
- In the low cycle fatigue regime, NiTi with retarded R-phase performs better up to the peak of stabilized strain of about 0.7%. Beyond 0.7% the R-phase transformation acts as a stress reliever, hence, improving low cycle fatigue of NiTi exhibiting the R-phase transformation.

### Fracture surfaces

- The size of fatigue fracture decreases progressively with decreasing number of cycles to rupture (Figs. 7 and 8). In terms of the percentage of the initial cross-section, the fatigue fracture size drops from 50% in the case of runout tests (1e6 cycles) down to 10% in the case of tests lasting few thousands of cycles.
- The fracture surface contains in general five distinct zones (Fig. 6) successively forming during fatigue crack growth as follows – 1. Fracture initiation at the surface; 2. Quasi-cleavage zone; 3. Fatigue striation zone; 4. Ductile fatigue crack zone; 5. Ductile final overload zone.
- Independently of the applied fatigue loading, the normal stress acting on the overload surface is higher than the stress needed for martensitic transformation to proceed (Fig. 9).

### Force-displacement hysteresis and fast thermography

- The last stage of the fatigue life lasting few tens of cycles is characterized by an unstable ductile fatigue fracture growth assisted by martensitic transformation proceeding massively and inhomogeneously within the gauge volume.
- In the last stage of the fatigue life, the martensitic transformation proceeding in the reduced cross-section dramatically decreases the resistance against the crack opening thus promoting high strains at the crack tip by far exceeding the reversible superelastic strains.
- Periodic localized phase transformation events probably arising from stress concentrating crack tips were spotted in 60% of the fatigue life.
- The periodic localized transformation events are believed to be linked to the steady crack growth marked with fatigue striations formation. At this stage, the crack growth is thus assisted by the martensitic transformation enhancing the crack opening that leads to large strains beyond superelastic limits.

### References

- [1] Van Humbeeck J. Shape memory alloys: a material and a technology. *Adv Eng Mater* 2001;3:837–50. doi: [http://dx.doi.org/10.1002/1527-2648\(200111\)3:11<837::AID-ADEM837>3.0.CO;2-0](http://dx.doi.org/10.1002/1527-2648(200111)3:11<837::AID-ADEM837>3.0.CO;2-0).
- [2] Yamauchi K, Ohkata I, Tsuchiya K, Miyazaki S. *Shape memory and superelastic alloys: applications and technologies*. Elsevier; 2011.
- [3] Otsuka K, Ren X. Physical metallurgy of Ti-Ni-based shape memory alloys. *Prog Mater Sci* 2005;50:511–678. doi: <http://dx.doi.org/10.1016/j.pmatsci.2004.10.001>.
- [4] Robertson SW, Pelton AR, Ritchie RO. Mechanical fatigue and fracture of Nitinol. *Int Mater Rev* 2012;57:1–37. doi: <http://dx.doi.org/10.1179/1743280411Y.0000000009>.
- [5] Mahtabi MJ, Shamsaei N, Mitchell MR. Fatigue of nitinol: the state-of-the-art and ongoing challenges. *J Mech Behav Biomed Mater* 2015;50:228–54. doi: <http://dx.doi.org/10.1016/j.jmbbm.2015.06.010>.
- [6] Kang G, Song D. Review on structural fatigue of NiTi shape memory alloys: Pure mechanical and thermo-mechanical ones. *Theor Appl Mech Lett* 2015;5:245–54. doi: <http://dx.doi.org/10.1016/j.taml.2015.11.004>.
- [7] Buehler WJ. Intermetallic compound based materials for structural applications. *Proc 7th navy sci symp solu NAVY prob adv technol*, vol. 1. Washington, D.C., USA: U.S. Naval Aviation Medical Center, Pensacola, Florida, USA: Office of Naval Research, Department of the Navy; 1963. p. 1–30.
- [8] Jackson CM, Wagner HJ, Wasilewski RJ. The alloy with a memory, 55-Nitinol: its physical metallurgy, properties, and applications. Battelle Memorial Institute; 1972.
- [9] Melton K, Mercier O. Fatigue of NITI thermoelastic martensites. *Acta Metall* 1979;27:137–44. doi: [http://dx.doi.org/10.1016/0001-6160\(79\)90065-8](http://dx.doi.org/10.1016/0001-6160(79)90065-8).
- [10] Melton KN, Mercier O. The effect of the martensitic phase transformation on the low cycle fatigue behaviour of polycrystalline NiTi and CuZnAl alloys. *Mater Sci Eng* 1979;40:81–7. doi: [http://dx.doi.org/10.1016/0025-5416\(79\)90010-7](http://dx.doi.org/10.1016/0025-5416(79)90010-7).
- [11] Kim Y. Fatigue properties of the Ti-Ni base shape memory alloy wire. *Mater Trans* 2002;43:1703–6. doi: <http://dx.doi.org/10.2320/matertrans.43.1703>.
- [12] Robertson SW, Stankiewicz J, Gong XY, Ritchie RO. Cyclic fatigue of Nitinol. In: SMST-2004 proc int conf shape mem superelastic technol. Baden-Baden Ger. ASM Intl Mater. Park OH; 2006. p. 79–88.
- [13] Kang G, Kan Q, Yu C, Song D, Liu Y. Whole-life transformation ratchetting and fatigue of super-elastic NiTi Alloy under uniaxial stress-controlled cyclic loading. *Mater Sci Eng A* 2012;535:228–34. doi: <http://dx.doi.org/10.1016/j.msea.2011.12.071>.
- [14] Figueiredo AM, Modenesi P, Buono V. Low-cycle fatigue life of superelastic NiTi wires. *Int J Fatigue* 2009;31:751–8. doi: <http://dx.doi.org/10.1016/j.ijfatigue.2008.03.014>.
- [15] Wagner M, Sawaguchi T, Kaistrater G, Höffken D, Eggeler G. Structural fatigue of pseudoelastic NiTi shape memory wires. *Mater Sci Eng A* 2004;378:105–9. doi: <http://dx.doi.org/10.1016/j.msea.2003.11.058>.
- [16] Gall K, Yang N, Sehitoglu H, Chumlyakov YI. Fracture of precipitated NiTi shape memory alloys. *Int J Fract* 2001;109:189–207. doi: <http://dx.doi.org/10.1023/A:101069204123>.
- [17] Creuziger A, Bartol L, Gall K, Crone W. Fracture in single crystal NiTi. *J Mech Phys Solids* 2008;56:2896–905. doi: <http://dx.doi.org/10.1016/j.jmps.2008.04.002>.
- [18] Rahim M, Frenzel J, Frotscher M, Pfetsching-Micklich J, Steegmüller R, Wohlschlägel M, et al. Impurity levels and fatigue lives of pseudoelastic NiTi shape memory alloys. *Acta Mater* 2013;61:3667–86. doi: <http://dx.doi.org/10.1016/j.actamat.2013.02.054>.
- [19] Racek J, Stora M, Šittner P, Heller L, Kopeček J, Petrenec M. Monitoring tensile fatigue of superelastic NiTi wire in liquids by electrochemical potential. *Shape Mem Superelast* 2015;1:204–30. doi: <http://dx.doi.org/10.1007/s40830-015-0020-5>.
- [20] Bertacchini OW, Lagoudas DC, Patoor E. Thermomechanical transformation fatigue of TiNiCu SMA actuators under a corrosive environment – part I: experimental results. *Int J Fatigue* 2009;31:1571–8. doi: <http://dx.doi.org/10.1016/j.ijfatigue.2009.04.012>.
- [21] Pelton AR. Nitinol fatigue: a review of microstructures and mechanisms. *J Mater Eng Perform* 2011;20:613–7. doi: <http://dx.doi.org/10.1007/s11665-011-9864-9>.
- [22] Robertson SW, Ritchie RO. A fracture-mechanics-based approach to fracture control in biomedical devices manufactured from superelastic Nitinol tube. *J Biomed Mater Res B Appl Biomater* 2008;84B:26–33. doi: <http://dx.doi.org/10.1002/jbm.b.30840>.
- [23] Maletta C, Sgambitterra E, Furgiuele F, Casati R, Tuissi A. Fatigue of pseudoelastic NiTi within the stress-induced transformation regime: a modified Coffin-Manson approach. *Smart Mater Struct* 2012;21:112001. doi: <http://dx.doi.org/10.1088/0964-1726/21/11/112001>.
- [24] Maletta C, Sgambitterra E, Furgiuele F, Casati R, Tuissi A. Fatigue properties of a pseudoelastic NiTi alloy: strain ratcheting and hysteresis under cyclic tensile loading. *Int J Fatigue* 2014;66:78–85. doi: <http://dx.doi.org/10.1016/j.ijfatigue.2014.03.011>.
- [25] Pelton AR, Dicello J, Miyazaki S. Optimisation of processing and properties of medical grade Nitinol wire. *Minim Invasive Ther Allied Technol* 2000;9:107–18. doi: <http://dx.doi.org/10.3109/13645700009063057>.

### Acknowledgment

We kindly acknowledge the financial support of this work provided by the Czech Science Foundation by projects No. 16-20264S, 14-15264S, 14-36566G. We further acknowledge city of Brest, France, for partly financing the PhD scholarship of Eduardo Alarcon. Microscopic observations were performed also thanks to the financial support provided by projects MEYS CR FUNBIO CZ.2.16/3.1.00/21568, LO1409 and LM2015088.

### Appendix A. Supplementary material

Supplementary data associated with this article can be found, in the online version, at <http://dx.doi.org/10.1016/j.ijfatigue.2016.10.005>.

- [26] Schaffer JE, Plumley DL. Fatigue performance of nitinol round wire with varying cold work reductions. *J Mater Eng Perform* 2009;18:563. doi: <http://dx.doi.org/10.1007/s11665-009-9363-4>.
- [27] Schaffer JE. Structure-property relationships in conventional and nanocrystalline NiTi intermetallic alloy wire. *J Mater Eng Perform* 2009;18:582–7. doi: <http://dx.doi.org/10.1007/s11665-009-9369-y>.
- [28] Reedlunn B, Daly S, Hector L, Zavattieri P, Shaw J. Tips and tricks for characterizing shape memory wire part 5: full-field strain measurement by digital image correlation. *Exp Tech* 2013;37:62–78. doi: <http://dx.doi.org/10.1111/j.1747-1567.2011.00717.x>.
- [29] Shaw JA, Kyriakides S. On the nucleation and propagation of phase transformation fronts in a NiTi alloy. *Acta Mater* 1997;45:683–700. doi: [http://dx.doi.org/10.1016/S1359-6454\(96\)00189-9](http://dx.doi.org/10.1016/S1359-6454(96)00189-9).
- [30] Iadicola MA, Shaw JA. The effect of uniaxial cyclic deformation on the evolution of phase transformation fronts in pseudoelastic NiTi wire. *J Intell Mater Syst Struct* 2002;13:143–55. doi: <http://dx.doi.org/10.1177/1045389022761402549>.
- [31] Sittner P, Liu Y, Novak V. On the origin of Lüders-like deformation of NiTi shape memory alloys. *J Mech Phys Solids* 2005;53:1719–46. doi: <http://dx.doi.org/10.1016/j.jmps.2005.03.005>.
- [32] Zheng L, He Y, Moumni Z. Effects of Lüders-like bands on NiTi fatigue behaviors. *Int J Solids Struct* 2016;83:28–44. doi: <http://dx.doi.org/10.1016/j.ijsolstr.2015.12.021>.
- [33] Miyazaki S, Otsuka K. Deformation and transition behavior associated with the R-phase in Ti-Ni alloys. *Metall Trans A* 1986;17:53–63. doi: <http://dx.doi.org/10.1007/BF02644442>.
- [34] Šittner P, Landa M, Lukáš P, Novák V. R-phase transformation phenomena in thermomechanically loaded NiTi polycrystals. *Mech Mater* 2006;38:475–92. doi: <http://dx.doi.org/10.1016/j.mechmat.2005.05.025>.
- [35] Nitinol 1 – Fort Wayne Metals; n.d.. <<http://www.fwmetals.com/services/resource-library/nitinol-1/>> [accessed September 18, 2016].
- [36] Šittner P, Heller L, Pilch J, Curfs C, Alonso T, Favier D. Young's modulus of austenite and martensite phases in superelastic NiTi wires. *J Mater Eng Perform* 2014;23:2303–14. doi: <http://dx.doi.org/10.1007/s11665-014-0976-x>.
- [37] Suresh S. *Fatigue of materials (Cambridge Solid State Science Series)*. 2nd ed. Cambridge; New York: Cambridge University Press; 1998.
- [38] Gollerthan S, Young ML, Neuking K, Ramamurti U, Eggeler G. Direct physical evidence for the back-transformation of stress-induced martensite in the vicinity of cracks in pseudoelastic NiTi shape memory alloys. *Acta Mater* 2009;57:5892–7. doi: <http://dx.doi.org/10.1016/j.actamat.2009.08.015>.
- [39] Cui J, Wu Y, Muehlbauer J, Hwang Y, Radermacher R, Fackler S, et al. Demonstration of high efficiency elastocaloric cooling with large  $\Delta T$  using NiTi wires. *Appl Phys Lett* 2012;101:73904. doi: <http://dx.doi.org/10.1063/1.4746257>.